Microplasma device architectures with various diamond nanostructures
Peer-reviewed author version

Microplasma devices architecture with various diamond nanostructures

Srinivasu Kunuku[1], Kamatchi Jothiramalingam Sankaran[2], Keh-Chyang Leou[1*]and I-Nan Lin[3*]

[1]Department of Engineering and System Science, National Tsing Hua University, Hsinchu 300, Taiwan, R.O.C

[2] Institute for Materials Research (IMO), Hasselt University, 3590 Diepenbeek, Belgium.

[3]Department of Physics, Tamkang University, Tamsui 251, Taiwan, R.O.C

Email: kcleou@ess.nthu.edu.tw, inanlin@mail.tku.edu.tw

Abstract: Diamond nanostructures (DNSs) were synthesized from three different morphological diamond, including microcrystalline diamond (MCD), nanocrystalline diamond (NCD), and ultrananocrystalline diamond (UNCD) films by RIE method and the plasma behavior of microplasma devices using the DNSs and diamond films as cathode materials were investigated. The Paschen-curve approach revealed that the γ-value of diamond materials is similar irrespective of the microstructure (MCD, NCD and UNCD) and geometry (DNSs and diamond films) of the materials. The diamond materials show markedly larger γ-coefficient than the conventional metallic cathode materials such as Mo and resulted in markedly better plasma illumination behavior for the corresponding microplasma devices. Moreover, the plasma illumination behavior, i.e., the voltage dependence of plasma current density (J_{pl}-V) and plasma density (n_e-V) characteristics and the robustness of the devices varied markedly with the microstructure and geometry of the cathode materials that is closely correlated with the EFE properties of the cathode materials. The UNCD nano-pillars, which possess the best EFE properties, resulted in markedly superior plasma behavior, whereas the MCD diamond films, which possess the worst EFE properties, led to inferior plasma behavior than the other kind of diamond cathode materials. Therefore, the detailed study

demonstrates that enhancement of plasma characteristics is due to collective effect of EFE behavior and secondary electron emission properties of cathode materials.

Keywords: diamond nanostructures, microplasma, electron field emission, secondary electron emission, plasma illumination.

1. Introduction

Micro-discharges have indispensable applications like plasma displays [7], tunable ultra-violet sources [9], spectroscopy of gases [10, 11], spectroscopy of water to study impurities [12], plasma treatment for materials and nanostructured arrays [13] and confined silicon etching processes [8]. Due to these potential applications, new area of research has been opened now to search for a cathode material, which can improve the plasma characteristics as well as enhance the long term sustainability of micro-discharges. High efficiency in generating secondary electrons via plasma ion bombardment (i.e., large γ-coefficient), which can improve the sustainability of micro-discharges, is of prime importance in the choice of the cathode materials for microplasma devices [15]. Diamond is one of the unique materials with high secondary electron emission coefficient γ-coefficient [14]. Moreover, diamond possesses outstanding properties like low sputtering yield due to its rigidity, high thermal conductivity and high chemical inertness, rendering these materials suitable for applications as cathode materials for microplasma devices. Diamond electrode has been employed as cathode in gas discharge light source for liquid crystal display backlighting [18, 19] and cathode in gas discharge tubes [20]. Recently, diamond films and their composites have been utilized in the fabrication of microplasma devices [21-26]. However, it is still not clear how the intrinsic characteristic of diamond such as its microstructure/geometry influenced the γ-coefficient of cathode materials, which in turn, enhanced the performance of the microplasma devices.

The estimation on γ-coefficient of cathode is an important task for designing the microplasma devices, as higher γ can give superior self-sustaining capability for the microplasma devices [16, 17].

Theoretical calculations and direct measurements of secondary electron yield by high energetic primary ion bombardment on materials can provide information on the intrinsic γ-coefficient of a material [27], but they do not predict how the microstructure and geometry of the cathode materials modified their γ-coefficient [28, 29]. In general, not only cathode's intrinsic properties but also its surface structure influences the secondary electron emission characteristics [30-32]. So it is of utmost importance to directly estimate the γ value by analyzing the discharge behavior of the plasma [33]. The well-known method called Paschen law, which was derived from Townscend theory, evaluated the γ-value of the cathode materials by using the electric breakdown properties of gases, such as minimum breakdown voltages (V_b) at optimum pressure × distance (*pd*)-value [34]. This technique is simple and effective for evaluating cathode materials in practical plasma environment.

In this study, we have synthesized diamond nanostructures (DNSs) from three different pristine diamond films via reactive ion etching (RIE) process. We have evaluated the γ-coefficient of these DNSs and diamond films by using Paschen curves approach and measured the microplasma properties such as voltage dependence of the plasma illumination (PI) and plasma density behaviors. The lifetime stability of these microplasma devices was also investigated to evaluate the robustness of these cathode materials.

2. Experimental methods

2.1. Cathode Materials

We fabricated three kinds of DNSs, such as microcrystalline diamond (MCD) nanocones, nanocrystalline diamond (NCD) nanotips and ultrananocrystalline diamond (UNCD) nanopillars from their respective diamond films. The fabrication process of DNSs is reported elsewhere [35]. Briefly, the pristine MCD, NCD and UNCD diamond films were first grown on Si substrates by using the microwave plasma enhanced chemical vapor deposition system (IPLAS, Cyrannus, 2.45 GHz), using $CH_4(1\%)/H_2$, $CH_4(1\%)/Ar(49\%)/H_2(50\%)$ and $CH_4(1\%)/Ar$ plasma, respectively. Prior to the reactive ion etching (RIE) process, Au thin film of 4 nm in thickness was deposited on pristine

diamond films, followed by annealing at 750°C to form self-assembled Au nanodots, which served as

a mask in the RIE process for fabricating the DNSs. These diamond films were then subjected to DC

biased RIE etching process in the presence of O_2 + CF_4 plasma. The fabricated DNSs were

characterized using field emission scanning electron microscopy (FESEM, JEOL-6500) and visible-

Raman spectroscopy (λ=632.8 nm, Lab Raman HR800, Jobin Yvon).

2.1. Microplasma devices

To investigate the effect of DNSs (or diamond films) cathode materials on the behavior of

microplasma devices, a cylindrical type microplasma device was made by using the DNSs (or

diamond films) as cathode and ITO/phosphor coated glass as anode, which were separated by

Teflon^{TM} spacer (~1 mm in thickness). A cylindrical cavity was formed by cutting a circular hole

(size ~5 mm) in Teflon spacer. The schematic diagram of microplasma measurement setup is shown

in figure 1. The devices were kept in the vacuum chamber with base pressure of 0.01 mTorr and

externally connected to DC power supply through a 500 kΩ resister. Prior to the measurements, all

the samples were heated at 200°C (1 hour) for removing the moisture on the surface to improve the

reliability of the measurements. Argon gas was allowed to flow at the rate of 10 sccm throughout the

measurements. The DC voltage was increased linearly from 0 V to the breakdown and then up to the

maximum voltage of 550 V for all the devices (at room temperature) and the plasma currents were

acquired at constant pressure. We have observed the plasma through transparent anode by USB

microscope and have taken the snapshots for different voltages to characterize the plasma

illumination (PI) behavior of the microplasma devices. The Microsoft paint was used to

quantitatively analyze of plasma illumination intensity, i.e., the RGB (RED+BLUE+GREEN) value,

of emission from the microplasma devices.

We have followed the conventional Paschen-curve method for estimating the γ values [36, 37].

The breakdown measurements were carried out for fixed electrode gap of 0.1 cm with the Ar gas

pressure varied from 0.1 to 10 torr and the breakdown phenomenon was monitored by measuring the

4

device current throughout process, while increasing the voltage monotonically. The breakdown voltage of the gas varied with pressure at the particular electrode gap. The lowest breakdown voltage at particular 'pd-value' was used to estimate the value of γ [36-39], that is, the breakdown parameters of Ar gas in all of these devices were used for calculating the γ by using equation (1).

$$\gamma = \frac{1}{e^{Apd\exp\frac{-Bpd}{V}} - 1} \tag{1}$$

where A, B are constants ($A = 0.09$ Pa^{-1} cm^{-1} and $B = 1.35$V Pa^{-1} cm^{-1} for Ar gas), V and pd are breakdown voltage and pd-value corresponding to lowest breakdown voltage (p is pressure and d= distance between electrodes).

3. Results

3.1 Material's characteristics

Figure 2 shows the SEM images of DNSs fabricated from different morphological diamond films and the SEM images of pristine diamond films are shown as insets in the corresponding figures. All these nanostructures (DNSs) are well aligned and uniformly distributed with high aspect ratios. These DNSs differ not only in the shape and number densities but also in granular structure. Figure 2 (a) illustrates the vertically aligned MCD nanocones, which were formed by RIE of MCD films, have geometry of a sharp pyramid and ~40 nm in size (measured in the base of pyramids are uniform). The size of each nanocones is markedly smaller than that of the grain size of MCD films, implying that each individual MCD nanocone was single crystalline as it was shaped from a faceted MCD grain. Each MCD diamond grain was converted into 4–5 MCD nanocones. Figure 2(b) shows the NCD nanotips of the size around tens of nanometers, which are of long rod geometry and are about the same size of diamond grains in NCD films (~ tens of nanometers, inset of figure 2(b)). Therefore, it seems that each nanotip is made by etching along a single NCD column. In contrast, figure 2(c) shows that the UNCD nanopillars are of totally different geometry from the MCD and

NCD DNSs. They are of blunt rod geometry and slightly larger in diameters than those of MCD (or NCD) derived DNSs. The UNCD diamond films consist of ultra-small spherical grains of the size around 5 nm and relatively thick grain boundaries, containing sp^2-bonded carbon [40]. Therefore, the UNCD nanopillars comprises of multiple diamond grains.

3.2 γ-coefficient of cathode materials

The most critical characteristic of the cathode materials, which influences the performance of the microplasma devices due to the efficiency of the cathode materials to emit secondary electrons due to the ion bombardment, i.e., the γ-coefficient. As it is well known that, while photoionization, radioactivity ionization and cosmic rays can initiate the breakdown phenomena in DC gas discharges, only the secondary electron emission from the cathode due to ion bombardment could make self-sustain the plasma [15-17]. Therefore, it is important to understand that how the granular structure and geometry of the cathode materials altered their γ coefficient. We utilized the Paschen-curves, which is the variation of breakdown voltage (V_b) against the pressure-distance product (pd-value), to evaluate the γ-coefficient of the DNSs and diamond films [36-39]. The Paschen curves of all the devices were measured at fixed cathode-to-anode distances (d = 0.1 cm) and are shown in figure 3(a) for DNSs and in figure 3(b) for diamond films, where the breakdown voltage (V_b) was measured with pressure varied from 0.1 Torr to 10 Torr. While increasing the pressure with step of 0.5 Torr at constant distance (d), the breakdown voltages first decreased with pressure, reaching a minimum value at $(pd)_{min}$, and then reverted back for higher pressure for all the materials. It is well known that, at lower *pd*-values than $(pd)_{min}$, the breakdown voltage is higher due to vacuum insulation and, at higher *pd*-values than $(pd)_{min}$, the breakdown voltage is higher due to high pressure insulation [36].

The Paschen-curve for MCD nanocones based devices is shown as curve I in figure 3(a), indicating that the V_b value decreased up to a minimum value of 349 V at $(pd)_{min} = 0.15$ Torr・cm

and then reverted back. By using these electric discharge parameters, we estimated the γ value from equation (1) as $(\gamma)_{MCD-DNSs} = 0.2327$ for MCD nanocones cathode materials. In contrast, the Paschen-curve of MCD film device was shown as curve I in figure 3(b) and the estimated γ value of $(\gamma)_{MCD\ film} = 0.2307$ was observed. It is surprising to see that the γ-value of MCD nanocones do not show much difference from that of MCD films. Such a phenomenon will be further discussed later. Similarly, for the case of NCD nanotips based devices, the minimum V_b value of 319 V occurred at lowest pd = 0.15 Torr $\cdot$ cm (curve II, figure 3(a)) with corresponding γ-value of $(\gamma)_{NCD-DNSs} = 0.2365$, whereas the Paschen curves corresponding to NCD films gives γ- values of $(\gamma)_{NCD\ film} = 0.2331$ (curve II in figure 3(b)), showing again that the γ-value does not change much when the morphology of the NCD materials changed from the nanotips to films. For the case of UNCD nanopillars based devices, the γ-values estimated from the Paschen curves in curve III of figure 3(a) is $(\gamma)_{UNCD-DNS} = 0.2384$, whereas for the case of UNCD films, the Paschen-curves in curve III of figure 3(b) show the γ-values of $(\gamma)_{UNCD\ film} = 0.2348$ for UNCD films device. To facilitate the comparison, the γ-value of Mo was also evaluated. The Paschen curve of Mo cathode is shown as curve IV in figure 3(b) for electrode gap of 0.1 cm, depicting the lowest breakdown voltage of 450 V at $(pd)_{min} = 0.20$ Torr $\cdot$ cm with γ-coefficient of $(\gamma)_{Mo} = 0.1224$, which is significantly smaller than those of diamond DNSs and diamond films. The γ-values of DNS, diamond films and Mo are tabulated in Table. 1.

It is interesting to notice that the γ-values of the cathode materials varied insignificantly among the diamond materials with the different granular structures (i.e., MCD, NCD or UNCD) and geometry (i.e., DNSs or films). However, the γ-values for diamond materials are markedly larger than Mo materials. These observations imply that the γ-value depends only on the material's intrinsic properties such as work function and ionization potential with the detailed microstructure and geometry of the materials showing insignificant effect. Such an observation is in accord with the proposed model [36].

3.3 The plasma illumination behavior

Knowing that all diamond cathode materials possess the same γ-coefficient, regardless of their granular structure and geometry, the effect of utilization of these DNSs and diamond films as cathode materials on the plasma characteristics of the microplasma devices were then investigated. Figure 4(a) shows the Ar plasma illumination characteristics of cylindrical type microplasma devices using the DNSs as cathode materials. Typical plasma illumination image of the microplasma devices are shown as inset in these figures. The plasma illumination intensities of these devices were evaluated in terms of total value of red (R) + green (G) + blue (B) [RGB] components of emission spectrum, which were plotted against the voltages in figure 4(a). The plasma illumination intensities of devices were measured at a distance of d = 5 cm away from the devices. These plots reveal that the plasma in the devices was triggered in the range of 290 - 350 V for DNSs cathode microplasma devices. The voltage at which the plasma of the devices was triggered was designated as "igniting voltage", V_i. The plasma intensity increases monotonously with voltage for all the devices after ignition. Among the three devices based on DNSs cathode materials, UNCD nanopillars based depict the highest plasma illumination intensity and MCD nanocones based devices exhibit the lowest intensity.

To better describe the plasma illumination behavior of these microplasma devices, the plasma current density (J_{pl})–voltage (V) curves for these devices at working pressure of 2 Torr were acquired. Figure 5(a) shows the J_{pl} –V curves for the microplasma devices using the DNSs as cathode materials, indicating the J_{pl} -values increased monotonously with applied voltages such as the J_{pl}-values emerge as 0.75 mA/cm^2 (for MCD), 0.92 mA/cm^2 (for NCD) and 1.50 mA/cm^2 (for UNCD) at an applied voltage of 430 V. Furthermore, the plasma density (n_e) was estimated from J_{pl} values of the plasma by using the Child's law (with Bohm sheath model), as shown in equation 2 [41].

$$n_e = \frac{J_{pl}}{eu_B} \tag{2}$$

Where e is the electron charge and u_B is the Bhom velocity. Bhom velocity of Ar ion is strictly dependent on the kinetic energy of the electron and the mass of ion, which is described in equation 3 [42].

$$u_B = \sqrt{\frac{kT_e}{m_i}} \tag{3}$$

Where k is the Boltzmann constant, T_e is electron temperature and m_i is the mass of Ar ion.

The T_e value of these typical plasma systems was evaluated from the optical emission spectrum (OES) of Ar plasma using Boltzmann plots. i.e., log (n_p/g_p) vs E_p, where n_p is the absolute populations of the different atomic levels of Argon, E_p is the energy of p level and g_p is the parity [43]. The n_p values were calculated from OES intensity I using eq. (4) [43].

$$I = \frac{hc}{4\pi} \frac{A_{pq}\Lambda_{pq}}{\lambda} n_p \text{------------------------------ (4)}$$

Where I is intensity of ArI lines, λ is the wavelength of the corresponding transition, h is the Planck's constant and c is the light velocity, A_{pq} is the coefficient for spontaneous emission from level p to level q and Λ_{pq} is the escape factor of this transition. The A_{pq} and Λ_{pq} values were acquired from the literature [43].

The OES spectrum of Ar plasma in MCD-nanocone based devices is shown in figure 5(b) and the inset shows the corresponding Boltzmann plot, which contains the (n_p/g_p) values corresponding to ArI lines (763.51 nm, 794.81 nm, 801.47nm and 840.82 nm) to illustrate the process for the evaluation of electron temperature (T_e) from the OES spectra. The slope of the Boltzmann plot illustrates the value of T_e as 7841 K (0.67 eV) for this plasma. By using the above mentioned formula (eqs. (2) and (3)), we have calculated the n_e-value corresponding to each measured J_{pl}-value in curve I of figure 5(a) and the n_e against the applied voltage (n_e–V) behavior are shown as curve I

in figure 5(c) for the MCD based DNSs devices. For the applied voltage of 430 V, the estimated n_e values is $(n_e)_{MCD-DNSs} = 3.92 \times 10^{16}$ m^{-3} for microplasma devices utilizing MCD nanocone as cathode. The OES spectra for NCD and UNCD based devices, which are not shown here, indicated that the T_e-values do not change much for different DNSs cathode materials, i.e., Te~7840 K. The NCD nanotip and the UNCD nanopillar based devices show the n_e-values as $(n_e)_{NCD-DNSs} = 4.79 \times 10^{16}$ m^{-3} and $(n_e)_{UNCD-DNSs} = 7.79 \times 10^{16}$ m^{-3} at an applied voltage of 430 V (curves II and III, figure 5(c), respectively). Among the DNSs-based microplasma devices, the UNCD nanopillar based devices exhibit the best performance, i.e., the lowest V_i-value with the largest n_e-value, whereas the MCD nanocones based devices exhibit the worst performance, i.e., the highest V_i-value with lowest n_e-values.

To facilitate the comparison, we also fabricated the microplasma devices using the three pristine diamond films, including MCD, NCD and UNCD films, as cathodes. Figure 4(b) shows the RGB-value of the plasma illumination and figure 6(a) shows the J_{pl} vs V curves for the pristine diamond films based microplasma devices, which indicates the igniting voltage, V_i-values, of 430 V for MCD films based devices, 400 V for NCD films based devices and 360 V for UNCD films based devices. The MCD film based devices reached the J_{pl}-value of $(J_{pl})_{MCD film} = 0.28$ mA/cm^2 (curve I, figure 6(a)) at an applied voltage of 460 V, whereas the NCD and the UNCD film based devices attained the J_{pl} values of $(J_{pl})_{NCD film} = 0.47$ mA/cm^2 and $(J_{pl})_{UNCD film} = 0.96$ mA/cm^2 (curves II and III, figure 6(a)), respectively. Similarly, the n_e-values of these devices were evaluated from the J_{pl}-value by using modified Child's law (i.e., eqs. (2) and (3)) and, at an applied voltage of 460 V, the n_e-values are lowest for MCD film based device $((n_e)_{MCD film} = 1.47 \times 10^{16}$/m^3, curve I, figure 6(b)). The n_e-values of NCD and UNCD film based devices are $(n_e)_{NCD film} = 2.48 \times 10^{16}$/m^3 (curve II, figure 6(b)) and $(n_e)_{UNCD film} = 4.99 \times 10^{16}$/m^3 (curve III, figure 6(b)), respectively. All these J_{pl}- and n_e-values were tabulated in Table. 2. Among the three pristine films based microplasma devices, the

10

UNCD films based devices exhibit the best, whereas MCD films based devices show worst plasma illumination behavior than other devices. Moreover, the DNSs based microplasma devices exhibits markedly superior better plasma illumination intensity to the diamond films based devices. Nevertheless, the diamond based microplasma devices based on either DNSs or diamond films based ones, show much better plasma performance compared with the Mo-based devices. The Mo based microplasma devices revealed higher igniting voltage (V_i-value) of 460 V with smaller J_{pl}-value (0.63 mA/cm^2, at 460 V, curve IV in figure 6(a)) and smaller n_e-value (3.27 $\times$ 10^{16} cm^{-3}, at 460 V, curve IV in figure 6(b)).

The EFE measurements of all the DNSs and diamond films are listed in Table. 3 [35], indicating that, among the DNSs, the UNCD nanopillars possess the best EFE properties, viz. with the lowest turn-on field (E_0=11.6 V/μm), the largest field emission enhancement factor (β=3041) and highest EFE current density (J_{efe}=3.95 mA/cm^2 at 3.0 V/μm), whereas the MCD nanocones possess the worst EFE performance, i.e., with the largest E_0 value (E_0=35.0 V/μm), the smallest β-factor (β=259) and the lowest J_{efe} (J_{efe}=0.91 mA/cm^2 at 200 V/μm). Moreover, the EFE properties of DNSs are markedly better than those of the diamond films. Comparison of Table. 2 and Table. 3 indicates that the superior the EFE properties of the cathode materials are, the better the performance of the microplasma devices. Restated, although all of DNSs and diamond films possess similar value of γ-coefficient, the DNSs-based microplasma devices do show better plasma performance compared with those of the diamond films-based ones that apparently can be ascribed to the superior EFE properties for DNSs cathode materials.

For practical application of plasma devices, not only the plasma illumination behavior but also the robustness of the microplasma devices is of great concern. Therefore, lifetime measurements were carried out for DNSs and diamond films based devices in order to investigate the robustness of these materials. The results of lifetime test of all the microplasma devices using these materials as

cathode are shown in the figure 7. This figure shows that, when measuring at an applied voltage of 450 V, the lifetime of $(\tau)_{MCD\ films}$ =6.17 h (at J_{pl} value of 0.4 mA/cm^2) was observed for MCD films based microplasma devices (curve I, figure 7(a)) and $(\tau)_{MCD\ nanocones}$ =4 h (at J_{pl} value of 1.1 mA/cm^2) for MCD nanocones based devices (curve II, figure 7(a)). The MCD films based microplasma devices exhibit longer lifetime than the MCD nanocone based devices. Notably, the larger J_{pl}-value was observed for MCD nanocones based devices as compared with that of the MCD films based devices, when tested under the same voltage, is due to the better EFE properties of the MCD nanocone cathode materials compared with those of the MCD films.

In contrast, for the case of NCD based microplasma devices, the lifetime values of $(\tau)_{NCD\ film}$ =5.35 h (at J_{pl} = 0.47 mA/cm^2) was achieved for NCD films based devices (curve I, figure 7(b)) and $(\tau)_{NCD\ nanotips}$ =3.75 h (at J_{pl} = 1.2 mA/cm^2) was attained for NCD nanotips based devices (curve II, figure 7(b)). The lifetime value of NCD based devices is slightly inferior to the MCD based ones, which is due to the presence of more abundant grain boundaries contained in NCD based cathode materials. However, the lifetime of NCD based devices are better than those of UNCD based devices. For the case of UNCD based devices, the τ -value measurements shows the lifetime of $(\tau)_{UNCD\ film}$ =4.7 h (at J_{pl} value of 0.85 mA/cm^2) for UNCD films based devices (curve I, figure 7(c)) and the τ-values of $(\tau)_{UNCD\ DNS}$ =2.9 h at J_{pl} = 1.7 mA/cm^2 (curve II, figure 7(c)) for UNCD nanopillars based devices. The lifetime measurements describe that the microplasma devices using diamond films as cathode exhibit longer lifetime than those using DNSs as cathode materials, which is expected.

The marked influence of granular structure of the diamond materials on the robustness of the materials is observed for the first time (i.e., $(\tau)_{MCD} > (\tau)_{NCD} > (\tau)_{UNCD}$). The possible explanation is that the MCD and NCD films (or the MCD nanocones and NCD nanotips) contain diamond grains with very sharp and clean grain boundaries, which are quite resistive to Ar ion bombardment damage. In contrast, the UNCD (or the UNCD nanopillars) contain ultrasmall diamond grains with abundant grain boundaries, which are relatively thick and contains sp^2-bonded carbons. The sp^2-bonded

carbons are much more susceptible to Ar ion bombardment damage that renders the UNCD (or the UNCD nanopillars) with markedly less robustness compared with the MCD and NCD films (or the MCD nanocones and NCD nanotips). The question that remained unexplained is why the cathode materials with superior EFE properties led to better performance of the corresponding microplasma devices.

4. Discussions

Simulation done by Venkatraman *et al.* [44-47] suggests that ion number density near the cathode causes the ion-enhancement in microelectromechanical devices. On the other hand, in the breakdown of a gas, usually termed Townsend's breakdown, there are two primary mechanisms that contribute to a significant rise in charge carriers – gaseous charge production through electron impact ionization (the α process) and cathode charge production through secondary emission (the γ process) [41, 47, 48]. Secondary emission is the electron emission from cathode materials due to bombarding particles/photons and is typically dominated by ions through Auger processes, though incident photons and metastable ions can also be a factor. Recent detailed experiments by Hourdakis *et al* [49] stated a mathematical model of the modified Paschen's curve, which investigated the role of surface protrusions in micro scale breakdown. These results showed that geometric surface enhancement was generally insufficient for the fields observed in breakdown experiments using conventional cathode materials such as copper or tungsten.

Higher γ-coefficient is apparently the major factor resulting in lower breakdown voltages and large enhancement in PI characteristics for microplasma devices using different DNSs (or diamond films) as cathode materials compared with those using Mo as cathode. However, our experimental studies on γ−coefficient for DNSs and diamond films show very slight variation in increase of γ−coefficient (4.3 %) among the cathode materials that cannot account for the lowest V_b-value and largest n_e-value of UNCD nanopillars based microplasma devices among the diamond based devices.

In contrast, the variation in J_{pl} (and n_e) values among the diamond based microplasma devices seems to be closely correlated with the EFE properties of the cathode materials (cf. Tables. 2 and 3). According to Fowler-Nordheim model [50], the EFE current density emitted from the cathode materials increased exponentially with the electric field experienced by the cathode after the EFE process of the materials was turned on:

$$J_e = \left(\frac{A\beta^2 E^2}{\varphi} \right) \exp\left(\frac{-B\phi^{\frac{3}{2}}}{\beta E} \right) \text{--- (6)}$$

where $A = 1.54 \times 10^{-6}$ A eV V^{-2} and $B = 6.83 \times 10^9$ eV$^{-3/2}$ V m^{-1}, β is the field-enhancement factor, E is the applied filed and φ is the work function of the emitting materials. However, for the cathode-to-anode separation of 1 mm in microplasma device, the electric field experienced by the diamond cathode materials is around 0.5 V/µm (when the applied voltage is 500 V), which is considerably smaller than the turn-on field required for triggering on the EFE process for the cathode materials (cf. Table. 3). Here, the only possible way of effect of EFE electrons in enhancing the plasma illumination behavior is in case of the post breakdown of Ar gas.

To understand such a possibility the plasma behavior of the microplasma devices in post breakdown process was investigated using CFD simulation, which is shown in supporting information. Briefly, from CFD simulations, it has been observed that, the electric field experienced by a cathode in post breakdown case increase dramatically compared with those prior to the breakdown process. Therefore, it can be concluded that the electrical fields experienced by the cathode materials in post breakdown process in microplasma devices will be sufficient for inducing the EFE process of the cathode materials. Therefore, both the larger γ-value and the superior EFE properties of DNSs (and pristine diamond films) renders these cathode materials behavior overwhelmingly superior to conventional Mo cathode materials thereby enhancing the PI performance of the microplasma devices.

5. Conclusion

The effect of cathode materials with different diamond nanostructures (DNSs) on enhancing the plasma illumination (PI) behavior of microplasma devices was systematically investigated. The DNSs include microcrystalline diamond (MCD) nanocones, nanocrystalline diamond (NCD) nanotips and ultrananocrystalline diamond (UNCD) nanopillars. The Paschen-curve measurements revealed that the diamond materials possess higher γ−value than the conventional metallic cathode materials such as Mo that led to enhanced plasma illumination (PI) behavior, i.e., lowered breakdown voltages with higher plasma density for the microplasma devices. However, different granular structure for the DNSs does not pronouncedly alter the γ-coefficient of the materials. On the other hand, the superior electron field emission (EFE) properties of cathode materials improved markedly the PI behavior of the microplasma devices. The microplasma devices using DNSs as cathode perform better than those which used diamond films as cathode materials. Among the different kind of DNSs, the UNCD nanopillars possess the best electron field emission properties and therefore, the corresponding microplasma devices exhibited the best plasma performance, compared to other kind of DNSs (or diamond films) used as cathode materials.

15

References:

[1] Thores J M and Dhariwal R S 1999 *Nanotechnology* **10** 102−107

[2] Dorai R and Kushner M J 2003 *J. Phys. D: Appl. Phys.* **36** 666-685.

[3] Callegari T, Ganter R and Boeuf J P 2000 *J. Appl. Phys.* **88** 3905−3913.

[4] Park S J, Chen J, Wagner C J, Ostrom N P, Liu C and Eden J G 2002 *IEEE J. Sel. Top. Quantum Electron*, **8** 387−394

[5] Park S J, Chen K F, Ostrom N P and Eden J G 2005 *Appl. Phys. Lett*. **86** 111501

[6] Mariotti D and Ostrikov K 2009 *J. Phys. D: Appl. Phys.* **42** 092002

[7] Yang S S, Lee J K, Ko S W, Kim H C and Shon J W 2004 *Contrib. Plasma Phys.* **44** 536−541

[8] Wang H, Li G, Jia L, Li L and Wang G 2009 *Chem. Commun.* **7** 3786−3788

[9] Kurunczi P, Lopez J, Shah H and Becker K 2001 *Int. J. Mass spectrum*. **205** 277−283

[10] Svensson T, Andersson M, Rippe L, Johansson J, Folestad S and Andersson-Engels S 2008 *Opt.Lett.* **33** 80−82

[11] Saito M, Hiraga T, Hattori M, Murakami S and Nakai T 2005 *Magn. Reson. Imaging,* **23** 607−610

[12] Que L, Wilson C G and Gianchandani Y B 2005 *J.Microelectromech. Syst.***14** 185−191

[13] Chakraborty A K and Golumbfskie A J 2001 *Annu. Rev. Phys. Chem.* **52** 537−573

[14] Pan L S and Kania D R 1995 Diamond: Electronic Properties and Applications Kluwer Academic, Boston.

[15] Tomio O, Tadashi S, Naoshi S, Mariko S, Hiroaki Y and Shuichi U 2006 *Diamond. Relat. Mater.* **15** 1998−2000

[16] Tadashi S, Tomio O, Naoshi S, Mariko S and Hiroaki Y 2007 *New Diam Front c tec* **17** 189−199

[17] Akimitsu H, Hiroshi N, Keishi Y and Tsuyoshi N 2007 *Plasma Process Polym.* **4** S942–S945

[18] Mitea S, Zeleznik M, Bowden M D, May P W, Fox N A, Hart J N, Fowler C, Stevens R and Braithwaite N StJ 2012 *Plasma Sources Sci. Technol.* **21** 022001

[19] Sankaran K J, Srinivasu K, Lou S C, Joji K, Chen H C, Lee C Y, Thai N H, Leou K C, Chen C C and Lin I N 2012 *Nanoscale res let* **7** 522

[20] Sankaran K J, Srinivasu K, Chen H C, Dong C L, Leou K C, Lee C Y, Thai N H and Lin I N *J. Appl. Phys.* **114** 054304

[21] Lou S C, Chulung C, Srinivasu K, Leou K C, Lee C Y, Chen H C, and Lin I N 2014 *J. Vac. Sci. Technol.,* B **32** 021202

[22] Tinghsun C, Srinivasu K, Sankaran K J, Leou K C, Tai N H and Lin I N 2014 *Appl. Phys. Lett.* **104** 223106

[23] Saravanan A, Huang B R, Sankaran K J, Srinivasu K, Dong C L, Leou K C, Tai N H and Lin I N 2014 *ACS Appl.Mater. Interfaces* **6** 10566−10575

[24] Yang S S, Lee S M, Iza1 F and Lee J K 2006 *J. Phys. D: Appl.Phys.* **39** 2775−2784

[25] Sobel A 1991 *IEEE Trans. Plasma Sci.* **19** 1032−1047

[26] Weston G F1975 *J. Phys. E: Sci. Instrum.* **8** 981− 991

[27] Hanson A L, Thieberger P, Steske D B, Zajic V, Zhang SY, and Ludewig H 2001 *J. Vac. Sci. Technol. A* **19** 2116–2121

[28] Loeb L B 1939 *Fundamental Processes of Electrical Discharges in Gases* J. Wiley and Sons, Inc., New York.

[29] Meek J M and Craggs J D 1953 *Electrical breakdown of gases* Oxford University Press.

[30] Lau S P, Huang L, Yu S F, Yang H, Yoo J K, An S J, and Yi G C 2006 *Small,* **2** 736–740

[31] Cheng Y H, Kupfer H, Richter F, Giegengack H, and Hoyer W 2003 *J. Appl. Phys.* **93** 1422−1427

[32] Aguilera L, Montero I, D´avila M E, Ruiz1 A, Gal´an L, Nistor V, Raboso D, Palomares J

and Soria F 2013 *J. Phys. D: Appl. Phys.* **46** 165104

[33] Auday G, Guillot Ph, Galy J   and Brunet H 1998 *J. Appl. Phys.* **83** 5917−5921

[34] Paschen F 1889 *Wied.* Ann. Phys., **273** 69−75

 [35] Srinivasu K, Sankaran K J, Tsai C Y, Chang W H, Tai N H, Leou K C and Lin I N 2013

ACS Appl. Mater. Interfaces **5** 7439−7449

[36] Raizer Y P 1991 *Gas Discharge Physics, Springer-Verlag*, New York.

[37] Braithwaite N St J 2000 *Plasma Sources Sci. Technol.* **9** 517−527

[38] Mariotti D, McLaughlin J A and Maguire J A 2004 *Plasma Sources Sci. Technol.* **13** 207−

212

[39] Auday G, Guillot Ph and Galy J 2000 *J. Appl. Phys,* **88** 4871−4874

[40] Wang C S, Chen H C, Cheng H F and Lin I N 2010 *J. Appl. Phys.* **107** 034304

[41] Lieberman M A, Lichtenberg A J 2005 2nd Edition; John Wiley & Sons:Hoboken, NJ.

[42] Chapman B 1980 Glow Discharge Processes sputtering and plasma etching John Wiley

& Sons, New York

[43] GarcιaU M C, Rodero A, Sola A and Gamero A 2000 *Spectrochimica Acta Part B* **55**

1733−1745

[44] Venkatraman V, Garg A and Peroulis D 2012 *Appl.Phys.Letts*, **100** 083503

[45] Walker D G, Harris C T, Fisher T S and Davidson J L 2005 *Diamond. Relat. Mater.* **14**

113−120

[46] Hourdakis E, Bryant G W and Zimmerman N M 2006 *J. Appl. Phys.* **100** 123306

[47] Venkattraman A 2015 Phys. Plasmas **22** 057102

Table **1**. Secondary electron emission coefficient (γ-coefficient) measurements at d = 0.1 cm in microplasma devices using these DNSs (or diamond films) as cathode

materials	V_b (V)		γ – vale	
	$(V_b)_{DNSs}$	$(V_b)_{films}$	γ_{DNS}	γ_{films}
MCD	349	373	0.2327	0.2307
NCD	319	348	0.2365	0.2331
UNCD	305	333	0.2384	0.2348
Mo bulk	-	450	-	0.1224

19

Table 2. **Plasma characteristics of the microplasma devices using diamond nano-structure (DNSs) or diamond films as cathode**

Sample name	J_{pl}-value at 460 V (mA/cm^2)		n_e-value at 460 V (10^{16} m^{-3})	
	$(J_{pl})_{DNSs}$	$(J_{pl})_{films}$	$(n_e)_{DNSs}$	$(n_e)_{films}$
MCD	0.80	0.32	3.92	1.60
NCD	1.01	0.50	5.00	2.55
UNCD	1.60	0.99	8.02	5.10
Mo bulk	-	0.63		3.27

Table 3. **Electron field emission properties of diamond nanostructures (DNSs) or diamond films**

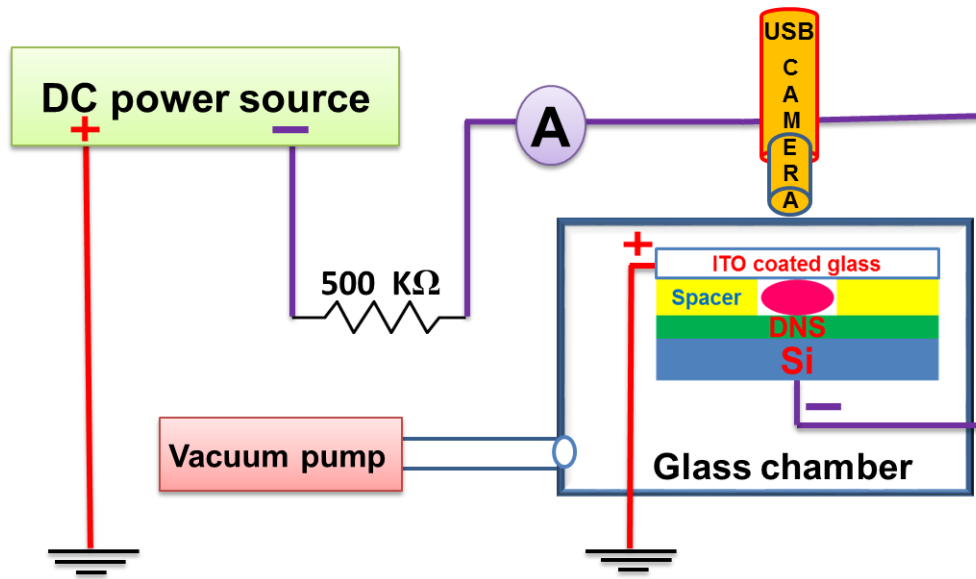| Sample name	E_0 (V/μm)		J_e (mA/cm^2)@ E_a (V/μm)		β – value	
	$(E_0)_{DNSs}$	$(E_0)_{films}$	$(J_e)_{DNSs}$	$(J_e)_{films}$	$β_{DNS}$	$β_{films}$
MCD	35.0	41.6	0.91@200	0.21@52.6	259	227
NCD	16.7	24	2.50@38	1.13 @ 35.2	347	309
UNCD	11.6	18.8	3.95@30	1.19 @ 28	3041	1191

20

Figure captions

Figure 1. Schematic diagram of microplasma measurement system.

Figure 2. SEM micrographs of (a) MCD nanocones, (b) NCD nanotips and (c) UNCD nanopillars. The insets show the corresponding SEM micrographs of the pristine diamond films used for fabricating the diamond nanostructures (the bar in the inset represents 200 nm).

Figure 3. Paschen-curves, the V_b vs. pd-value, of microplasma devices, which used (a) DNSs and (b) diamond films as cathode materials.

Figure 4. Variation of RGB values against applied voltage for microplasma devices using (a) DNSs and (b) diamond films as cathode materials. The RGB values estimated at source to USB camera distances of 5 cm and the insets show the corresponding plasma illumination images.

Figure 5. (a) J_{pl} vs. V characteristics and (c) n_e vs. V characteristics of the microplasma devices using DNSs as cathode: (I) MCD nanocones, (II) NCD nanotips and (III) UNCD nanopillars; (b) OES spectrum of typical microplasma devices using DNSs of MCD as cathode at pressure of 2 torr and applied voltage of 500 V with inset showing the Boltzmann plot.

Figure 6. (a) J_{pl} vs V characteristics and (b) the n_e vs V characteristics of microplasma devices using diamond films as cathode : (I) of MCD films, (II) NCD films, (III) UNCD films and (V) Mo bulk.

Figure 7. Lifetime measurements of microplasma devices operated under applied voltage of 450 V and working pressure of 2 torr: (a) MCD based devices, (b) NCD based devices and (c) UNCD based devices at applied voltage of 450 V. The (I)'s for diamond films and (II)'s for DNSs.

1
2
3
4
5
6
7
8
9
10
11
12
13
14
15
16
17
18
19
20
21
22
23
24
25
26
27
28
29
30
31
32
33
34
35
36
37
38
39
40
41
42
43
44
45
46
47
48
49
50
51
52
53
54
55
56
57
58
59
60

Figure S1. CFD simulated curves of (a) potential distribution (b) electric field distribution (c) plasma density distribution and (d) ion density distribution of DC plasma between two electrodes at pressure of 0.4 torr and voltages of 500 V and 600 V. The dotted lines show the curves for Mo case ($\gamma = 0.1224$) and the solid lines show the curves for diamond case ($\gamma = 0.2433$).

Figure S2. CFD contour plots of (a) potential distribution; (b) electric field distribution, (c) plasma density distribution and (d) Ar^{+} ion density distribution of DC plasma between two electrodes at pressure of 0.4 torr and voltages of   600 V.

1
2
3
4
5
6
7
8
9
10
11
12
13
14
15
16
17
18
19
20
21
22
23
24

Figure 1. Schematic diagram of microplasma measurement system.

25
26
27
28
29
30
31
32
33
34
35
36
37
38
39
40
41
42
43
44
45
46
47
48
49
50
51
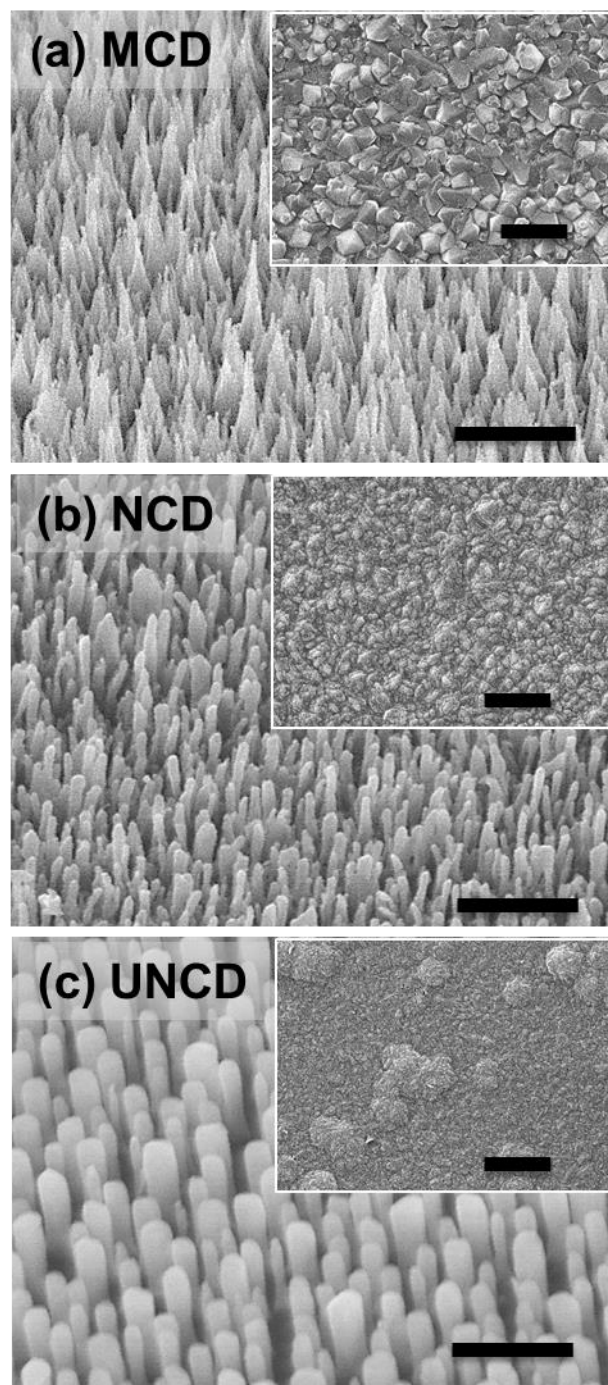52
53
54
55
56
57
58
59
60

Figure 2. The SEM micrographs of (a) MCD nanocones, (b) NCD nanotips and (c) UNCD nanopillars. The insets show the corresponding SEM micrographs of the pristine diamond films used for fabricating the diamond nanostructures (the bar in the inset represents 200 nm).
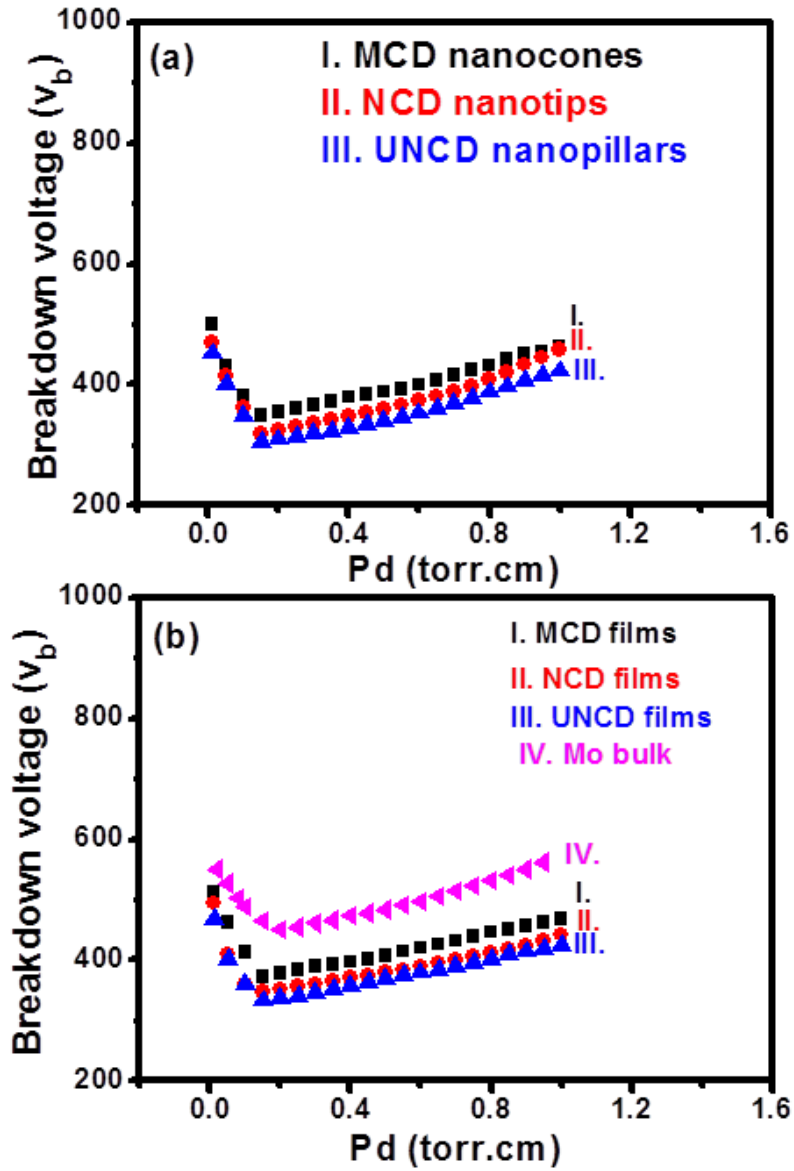
Figure 3. Paschen-curves, the V_b vs. pd-value, of microplasma devices, which used (a) DNSs and (b) diamond films as cathode materials.
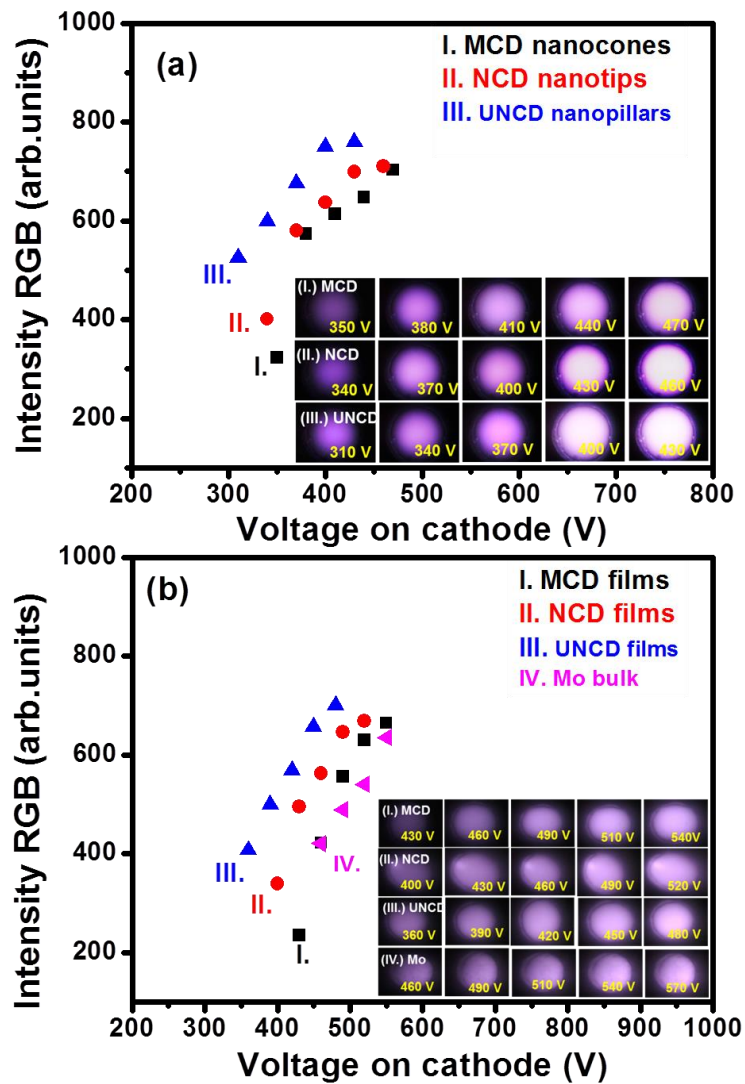
Figure 4. The variation of RGB values against applied voltage for microplasma devices using (a) DNSs and (b) diamond films as cathode materials. The RGB values estimated at source to USB camera distances of 5 cm and the insets show the corresponding plasma illumination images.
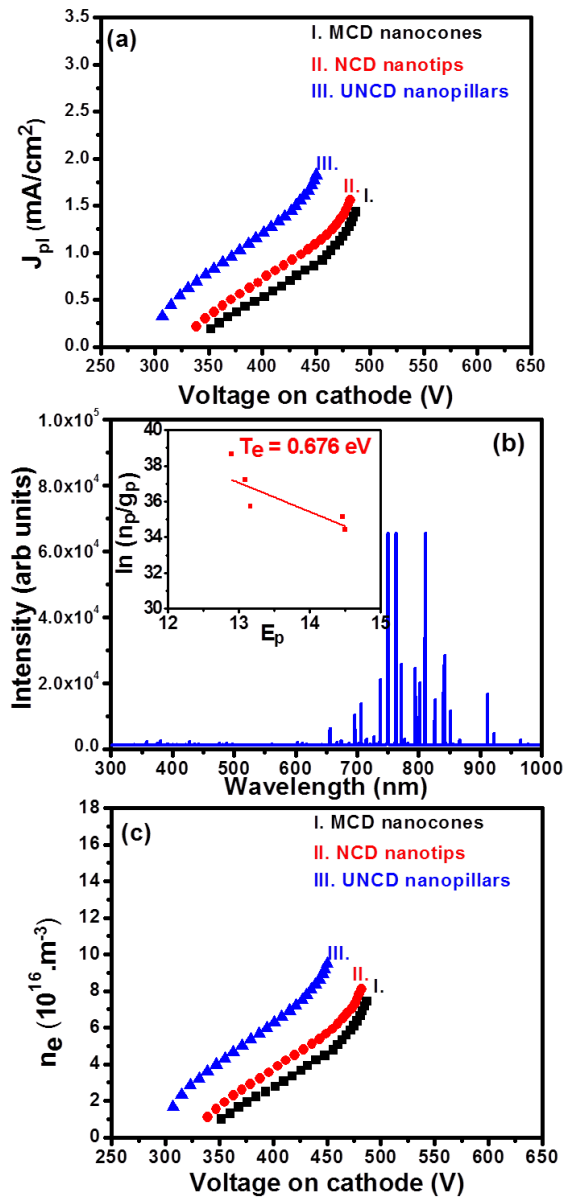
26

Figure 5. (a) The J_{pl} vs. V characteristics and (c) The n_e vs. V characteristics of the microplasma devices using DNSs as cathode: (I) MCD nanocones, (II) NCD nanotips and (III) UNCD nanopillars; (b) OES spectrum of typical microplasma devices using MCD DNSs as cathode at pressure of 2 torr and applied filed of 500 V with inset showing the Boltzmann plot.
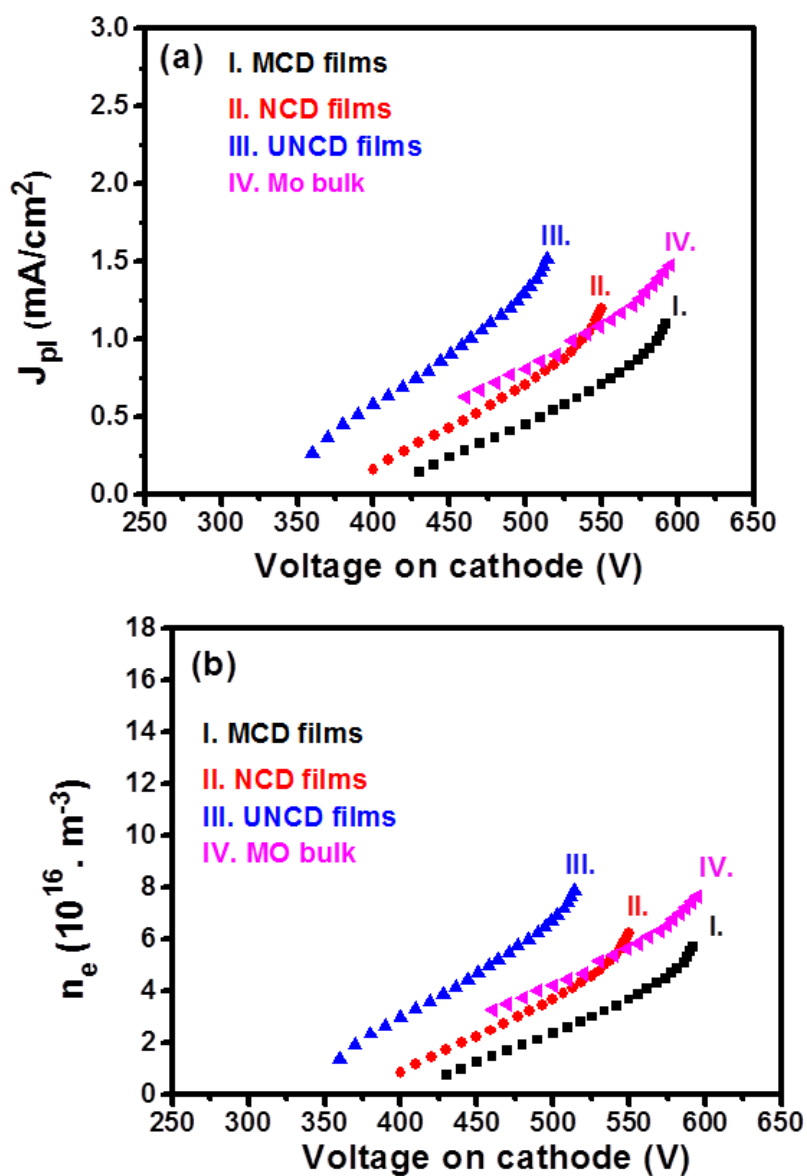
27

Figure 6. (a) The J_{pl} vs V characteristics and (b) the n_e vs V characteristics of microplasma devices using diamond films as cathode : (I) of MCD films, (II) NCD films, (III) UNCD films and (V) Mo bulk.
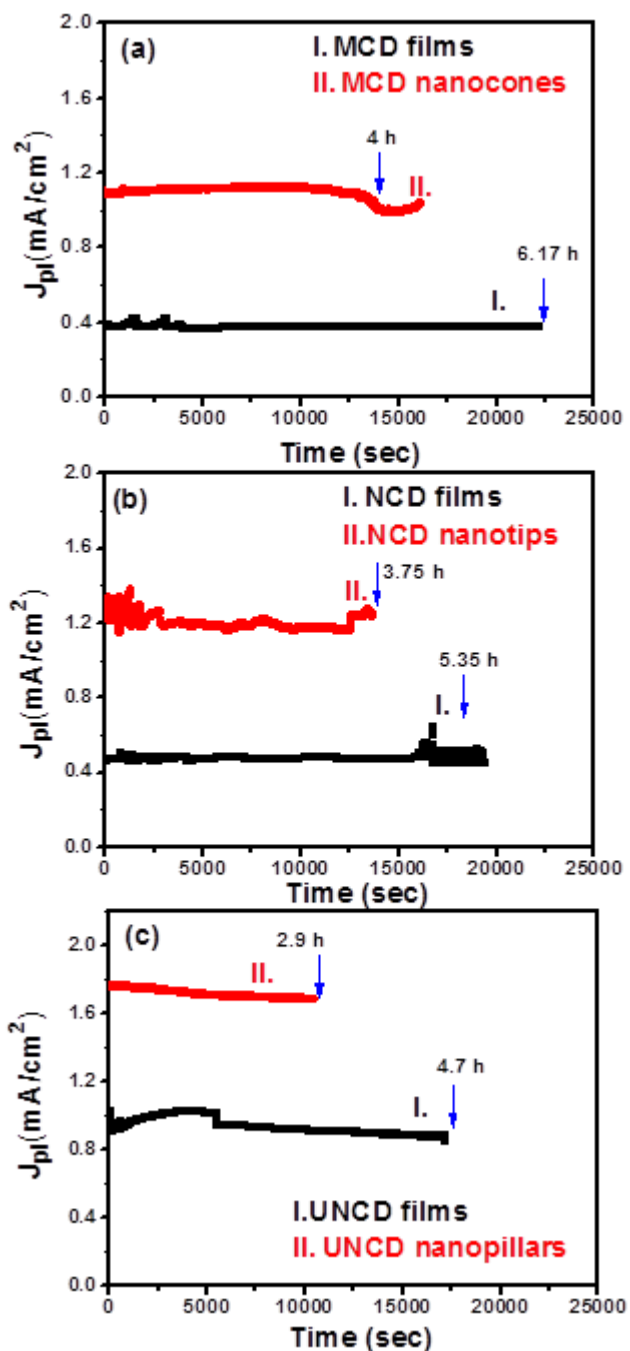
Figure 7. The lifetime measurements of microplasma devices operated under applied voltage of 450 V and working pressure of 2 torr: (a) is for MCD based devices, (b) NCD based devices and (c) UNCD based devices at applied voltage of 450 V. The (I)'s for diamond films and (II)'s for DNSs.